Doped photo-crosslinked polyesteramide hydrogel as solid electrolyte for supercapacitors

Guillem Ruano,[1] Jordi Tononi,[1] David Curcó,[2] Jordi Puiggalí,[1,3] Juan Torras,[1,*] and Carlos Alemán[1,3,*]

[1] *Departament d'Enginyeria Química and Barcelona Research Center for Multiscale Science and Engineering, EEBE, Universitat Politècnica de Catalunya, C/ Eduard Maristany, 10-14, 08019, Barcelona, Spain*

[2] *Departament d'Enginyeria Química i Química Analítica, Facultat de Química, Universitat de Barcelona, Martí i Franquès 1, Barcelona E-08028, Spain*

[3] *Institute for Bioengineering of Catalonia (IBEC), The Barcelona Institute of Science and Technology, Baldiri Reixac 10-12, 08028 Barcelona Spain*

Correspondence to: joan.torras@upc.edu and carlos.aleman@upc.edu

Abstract

High-performance hydrogels play a crucial role as solid electrolytes for flexible electrochemical supercapacitors (ESCs). More specifically, all solid-state ESCs based on renewable, biodegradable and/or biocompatible hydrogels doped with inorganic salts as electrolytes are attractive not only because of their contribution to reduce the resource consumption and/or the generation of electronic garbage, but also due to their potential applicability in the biomedical field. Here, computer simulations have been combined with experimental measurements to probe the outstanding capability as solid electrolyte of photo-crosslinked unsaturated polyesteramide hydrogels containing phenylalanine, butenediol and fumarate, and doped with NaCl (UPEA-Phe/NaCl). Atomistic molecular dynamics simulations have shown the influence of the hydrogel pore structure in Na^+ and Cl^- ions migration, suggesting that UPEA-Phe/NaCl hydrogels prepared without completing the photo-crosslinking reaction will exhibit better behavior as solid electrolyte. Theoretical predictions have been confirmed by potentiodynamic and galvanostatic studies on ESCs fabricated using poly(3,4-ethylenedioxythiophene) electrodes and UPEA-Phe/NaCl hydrogels, which were obtained using different times of exposure to UV radiation (*i.e.* 4 and 8 h for uncomplete and complete photo-crosslinking reaction). Moreover, the behavior as solid electrolyte of the UPEA-Phe/NaCl hydrogel prepared using a photo-polymerization time of 4 h has been found to be significantly superior to those exhibited by different polypeptide and polysaccharide hydrogels, which were analyzed using ESCs with identical electrodes and experimental conditions.

Introduction

Among modern flexible and wearable energy storage devices, compressible, stretchable and bendable electrochemical supercapacitors (ESCs) show great potential for practical applications because of its high power density, environmental friendliness, safety, fast rate of charging-discharging and long cycling lifetime.[1-6] Flexible ESCs require that all device components, the electrodes and the electrolyte, to be flexible. In the last few years a huge amount of work has been devoted to develop and characterize flexible electrodes.[7-14] Besides, polymeric hydrogels have attracted increasing attention as flexible electrolytes because of their minimum leakage compared to liquid electrolytes and relatively high ionic conductivity, especially when compared to solid polymers.[15-21]

Polymer hydrogel electrolytes have been prepared using synthetic polymers, as for example polyvinyl alcohol[15-18] and polyacrylic acid.[19,20] However, in recent years the utilization of hydrogels based on biopolymers from biomass and/or synthetic biopolymers based on natural constituents is gaining more attention.[21-35] These bio-based solid electrolytes exhibit important advantages, for instance renewability, earth abundancy, low-cost, biodegradability, biocompatibility and/or environmental friendless. Thus, fabrication of bio-based electrolytes contributes to reduce not only the resource consumption but also the enormous electronic garbage after their service lifetime.

In the last few years we have been interested in the development of solid electrolytes for ESCs based on natural polysaccharides, such as κ-carrageenan[31,32] and cellulose,[33] and on synthetic biopolymers, as for example poly-γ-glutamic acid[34] and phenylalanine-containing unsaturated polyesteramides (UPEAs).[35] Interestingly, a photo-crosslinked UPEA hydrogel containing phenylalanine, butenediol and fumarate as building blocks and doped with NaCl

(UPEA-Phe/NaCl), exhibited better behavior as supporting electrolyte than biohydrogels derived from polysaccharides and polypeptides doped with same salt, without any detriment in the biodegradability and biocompatibility.[35]

Studies on polysaccharides and polypeptides showed that the performance of biohydrogels as solid electrolytes is known to depend on the porous structure.[33,34] Thus, systems with large inter-connected pores were found to favor the transport of ions, exhibiting better response. Key in the control of the pore architecture and network structure is the synthesis of the hydrogel (*e.g.* regulating the concentration of polymer : crosslinker agent ratio or using templates). However, in the case of photo-crosslinked UPEAs this is expected to be done by adjusting the photo-polymerization time (*i.e.* the time of exposure to UV radiation). In this work we employ a synergistic strategy based on both computational molecular dynamics (MD) simulations and experimental approaches to optimize the properties of the UPEA-Phe/NaCl as solid electrolyte. More specifically, atomistic MD simulations have been conducted to investigate the effect of the pore structure in ions migration. Computational results have been used to reduce the photo-polymerization time from 8 h to 4 h, enhancing significantly the response of UPEA-Phe/NaCl as solid electrolyte, which has been proved by comparing key performance parameters. Our approach demonstrates that UPEA-Phe/NaCl hydrogel electrolyte could be used for manufacturing efficient flexible ESCs.

Results and Discussion

Computational modeling

UPEA-Phe hydrogel is synthesized by photo-crosslinking the unsaturated bonds of UPEA-Phe chains with poly(ethylene glycol) (PEG), which is previously functionalized with unsaturated bonds to act as crosslinker (Scheme 1):[35]

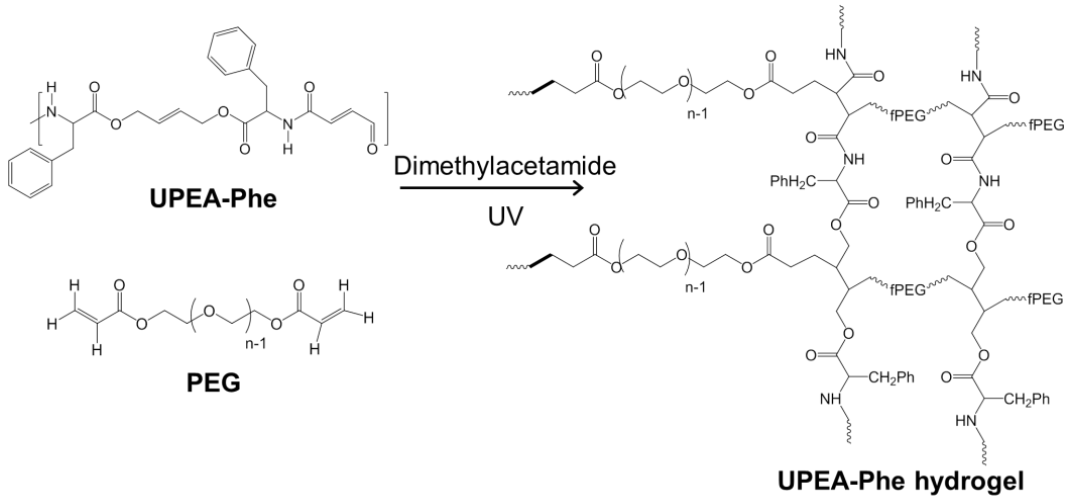

Scheme 1. Photopolymerization reaction to produce UPEA-Phe hydrogel

The pore size, which is controlled by the crosslinking degree (CLD) that in turn is regulated by the time of exposure to UV radiation, is expected to have a major effect on the properties of the hydrogel. In particular, its capacity to transport Na^+ and Cl^- ions when the doped UPEA-Phe/NaCl hydrogel is used as solid electrolyte in ESCs. In this section, the influence of the structure of the hydrogel on the diffusion of Na^+ and Cl^- ions in UPEA-Phe/NaCl has been studied using atomistic MD simulations. Three different variables have been considered for the simulations: the electric field (EF), the cross-linking degree CLD) and the hydration degree (HD).

Unfortunately, the construction of crosslinked polymeric models (*i.e.* starting configurations for MD) using conventional simulation techniques is very hard and inefficient because of the following adversity: a dense and heterogeneous distribution of

atoms with well-defined the connectivity for both the backbone and the crosslinks (*i.e.* bond lengths and bond angles).[36,37] In order to overcome such adversity, which involves severe restraints, the utilization of specifically designed approaches is necessary. Nonetheless, the length- and time-scales of polymer dynamics, which are unaffordable by such approaches, drastically restricts the efficacy of simulation algorithm that are subjected to strong geometric restrictions.[36,37] For example, UPEA-Phe and functionalized PEG require a photocrosslinking time of at least 6 h (see below) to reach a very high CLD. Thus, the dynamics of the system throughout this period allow all (or almost all) reactive sites to be close enough for photoreaction. This spatial coincidence cannot be achieved using current simulation algorithms and computational facilities, preserving the connectivity distribution (*i.e.* bond lengths and bond angles of both the main chain and crosslinks at the right values), due to the scale. These strong limitations can be solved by focusing the problem on the realistic representation of a single aspect of the system to be studied, and neglecting the rest of the aspects. In this work we focused simulations on the effect of the size of the pores in the transport ions, neglecting other aspects that depend on the dynamics of the polymer chains as for example the evolution of the hydrogel structure with the photocrosslinking time.

Three different hydrogel models were built using an early developed strategy that was engineered to construct reliable 3D molecular architectures of hydrated crosslinked materials.[38] More specifically, this methodology was designed to generate and relax molecular microstructures of crosslinked systems, respecting the connectivity of the molecular system (in the case of UPEA-Phe hydrogel is given by the formula displayed in Scheme 1) and imposing the CLD. In brief, this strategy consists on the following four-step algorithm:

1) The positions of the atoms of the first UPEA-Phe unit were generated within the simulation box using an algorithm that was designed to provide conformations with minimum torsional strains and without repulsive non-bonded interactions.[39,40] Then, a Monte Carlo criterion was applied to choose one of the following three options: (i) the second UPEA-Phe repeat unit was generated at the left side of the first one; (ii) the second UPEA-Phe repeat unit was generated at the right side of the first one; and (iii) a PEG chain was generated to form a crosslink.
2) If option (i) or (ii) are selected in step 1), the second UPEA-Phe repeat unit is generated without steric overlaps. If option (iii) was chosen in the previous step, both a position of the first UPEA-Phe repeat unit and a position of the second UPEA-Phe repeat unit, are randomly chosen among those able to form crosslinks (*i.e.* those corresponding to unsaturated bonds) to generate the PEG chain. Then, a number of PEG repeat units, m_1, comprised between 25 and 50 is randomly chosen. The cross-link is considered as feasible when the atomic positions generated for the $(PEG)_{m1}$ chain do not overlap with previously generated atoms, whereas a new number of PEG repeat units, m_2 ($m_2 > m_1$) is randomly selected again if steric overlaps are detected. If after five trials, the generation of the crosslink fails, the algorithm comes back to step 1). Independently of the option, the positions of the atoms contained in the second UPEA-Phe repeat unit or the PEG crosslinker are obtained one-by-one.
3) The rest of the UPEA-Phe repeat units and PEG chains are generated one-by-one using the procedure. The following features are distinctive of this repetition process: (a) at the end of the generation process, the number of crosslinks is the whole

system must be equal to the fixed CLD; and (b) the geometry of the connectivity (*i.e.* bond lengths and bond angles) must be respected in all cases.

Three models with 240 UPEA-Phe repeat units each and CLDs of 17%, 25% and 35%, which correspond to 40, 60 and 86 PEG chains, respectively, were generated using such strategy. The average number of repeat units per PEG crosslink in these systems was 42, 47 and 43, respectively. Models for CLD= 17%, 25% and 35% contained 27685, 36879 and 43677 explicit atoms, respectively. The homogeneous and relatively compact distribution of polymer chains found for the model without crosslinks transforms into a heterogeneous distribution due to the positional (functionalized PEG chains react with the double bonds of butenediol and fumarate units) and geometric (bond lengths and bond angles according to the connectivity) restraints introduced by the crosslinks. Thus, the crosslinks induced the formation of pores with ellipsoidal-like shapes, as is reflected in the models depicted in Figure 1. The pore size (PS) was determined by averaging at least 30 different diameters (including the major and the minor) at the surface of each pore and, subsequently, averaging the values found for the pores of 40 different stored snapshots separated by 2.5 ns intervals. The PS was 25±6, 39±11 and 58±14 Å for the model with a CLD of 17%, 25% and 35%, respectively, indicating that the size of the pores increases with the CLD. Obviously, this increasing effect is expected to occur until a threshold value of the CLD only, the dimensions of the pore decreasing when the number of crosslinks is very high because of the severe geometric constrictions. Unfortunately, reliable models with a CLD higher than 35-40% are not feasible using current computational strategies. Besides, inspection to the distributions of the measured diameters, which are included in Figure 1,

reveals two peaks in all cases, which is fully consistent with the ellipsoidal-like geometry of the pores.

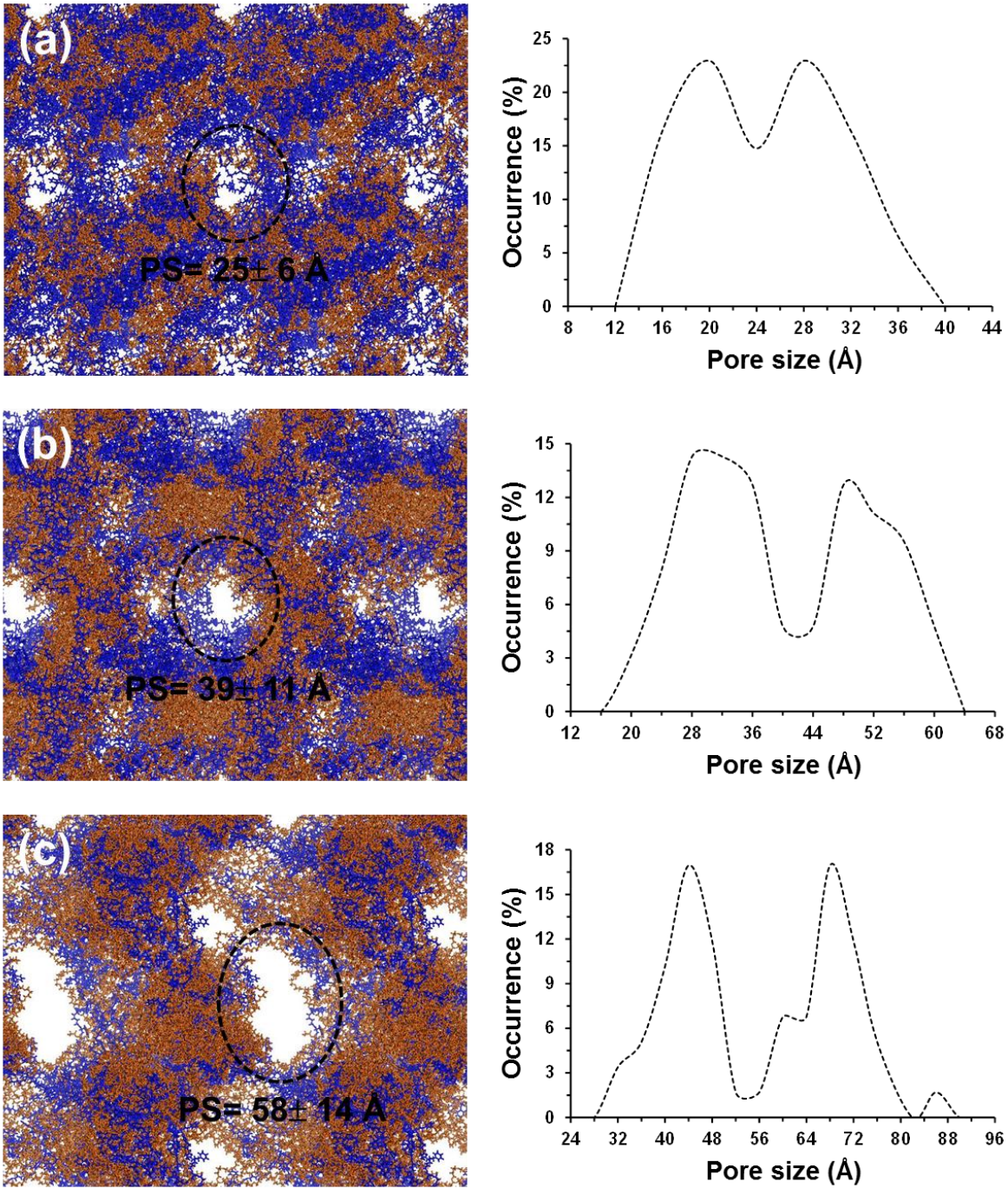

Figure 1. Models for UPEA-Phe hydrogel constructed with different CLDs: (a) 17%, (b) 25% and (c) 35%. Blue and orange chains correspond to the UPEA backbone and PEG cross-linkers, respectively. In order to provide a clearer visualization of the pores, parts of

the neighboring periodic cells have been included in the images. The averaged value of the pore size (PS) is displayed for each model. The distribution of pore sizes as measured for 20 different stored snapshots separated by 5 ns intervals are displayed for each model (right).

Then, the three models were hydrated by introducing water molecules, which were randomly incorporated at positions not occupied by the polymer atoms.[38] For each model, three different hydration degrees (HDs) were considered: 100% w/w, 300% w/w and 500% w/w. The exact number of explicit water molecules used for each model, which depends on the CLD, is provided in Table S1. Also, Na^+ and Cl^- ions were added to reach a 0.1 M NaCl concentration. The number of Na^+ and Cl^- ions added to each system is included in Table S1. Accordingly, the total number of explicit atoms for the nine simulated models (3 CLDs × 3 HDs with 0.1 M NaCl) ranged from 47,901 (CLD= 17%, HD= 100% w/w) to 285,399 (CLD= 35%, HD= 500% w/w).

After their thermalization and equilibration using the protocol described in the ESI, the nine constructed models were used as starting points for independent production MD simulations, which were conducted considering the following electric fields (EF): 0.0, 20, 40, 80 and 160 V/mm. The EF was fixed along the *z*-axis of the simulation box, the force on each atom, *i*, of the model ($\mathbf{F'_i}$) being defined by the following expression:

$$\mathbf{F'_i} = \mathbf{F_i} + q_i \cdot \mathbf{E_z} \qquad (1)$$

where $\mathbf{F_i}$ is the force defined by the potential force-field (*i.e.* the GAFF force-field[41,42] was used for this study), q_i is the charge of the atom *i*, and $\mathbf{E_z}$ is the EF. It is worth noting that the utilization of a fixed model, which successfully describes the transport of simple ions, allows a dramatic reduction in computational cost compared to polarizable models.[43,44] A

total of 45 production MD runs (9 models × 5 EFs), each of 200 ns, were conducted, which represent a total simulation time of 9 μs.

All simulations were run using the Amber18 package,[45] computational details about the procedures being described in the ESI. The structure of the modeled hydrogels did not experienced significant changes since they are considerably restrained by the crosslinks. For example, simulations using the largest electric field (EF= 160 V/mm) showed that the averaged pore size experienced a variation of 8%, 5% and 4% with respect to simulations without electric field for the systems with CLD= 17%, 25% and 35%, respectively.

The diffusion coefficient (*D*) of Na^+ and Cl^- ions was calculated using the Einstein relation:

$$D = \frac{1}{6n}\lim_{t\to\infty}\frac{d}{dt}MSD \qquad (2)$$

where *t* is time, *MSD* is the mean square displacement and *n* is the number of cations or anions. Eq (2) is only valid when the Einstein diffusive regimen is reached (*i.e.* the motion of the diffusing ions follows a random walk; in other words, their motion is not correlated with their motion at any previous time). Inspection of the temporal evolution of the *MSD* (see below) reflected an anomalous diffusion for a short period of time (ranging from ~30 ns to ~80 ns) before to reach the diffusive regime. This part of the trajectory was excluded from the diffusion analyses. Thus, after the anomalous diffusion period, the *MSD* of the diffusing particles increases linearly with time and the slope, *m*, of such curve is 1.0 (*i.e.* accelerated and anomalous diffusive regimes exhibit $m < 1$ and $m > 1$, respectively[46]).

Figures 2a and 2b represent the variation of *D* for Na^+ and Cl^- (D_{Na+} and D_{Cl-}, respectively) against the EF for UPEA-Phe/NaCl with CLD= 17%, 25% and 35% and HD= 100%, while Figure S1 shows the temporal evolution of MSD for a representative system

(UPEA-Phe/NaCl with CLD= 17% and HD= 100%) using the different EFs. As is shown, the diffusion of the two ions does not follow any trend with respect to the EF variation in the studied range. Thus, the influence of the chemical structure of the hydrogel on D_{Na+} and D_{Cl-}, which range from $0.13 \cdot 10^{-5}$ (CLD= 17%) to $0.36 \cdot 10^{-5}$ cm^2/s (CLD= 35%) and from $0.20 \cdot 10^{-5}$ (CLD= 17%) and $0.49 \cdot 10^{-5}$ cm^2/s (CLD= 35%), respectively, is much higher than that of strength of the EF. Similarly, the effect of the EF on D_{Na+} and D_{Cl-} was practically inexistent for doped hydrogels with HD= 300% and 500% (Figure S2).

On the other hand, Figures 2 and S2 show that D_{Cl-} is higher than D_{Na+} for all the studied CLDs and HDs. This has been attributed to the interaction between the Na^+ ions and the oxygen atoms from carbonyl groups of the UPEA-Phe backbone. The strength of this interaction is illustrated is Figure 3a, which displays the radial distribution functions (RDFs) for $Na^+ \cdots O2$ atoms pair (O2 refers to the first oxygen atom of the fumarate unit, Scheme S1). The profiles obtained for hydrogels with CLD= 17%, 25% and 35% and HD=100% display a sharp and intense peak at a distance r= 2.3 Å. The intensity of this peak decreases with increasing CLD, reflecting that crosslinks hinder the access of Na^+ to the oxygen atoms of the fumarate units. Identical conclusions are reached by inspecting the RDFs involving the $Na^+ \cdots O8$, $Na^+ \cdots O28$ and $Na^+ \cdots O42$ atom pairs (Figure S3), where O8, correspond to the oxygen atom of the second carbonyl of the fumarate unit and O28 and O42 refer to the oxygen atom of first and second Phe units (Scheme S1), respectively. Instead, no peak is observed in the RDFs involving Cl^- ions, explaining why their mobility is superior to that of Na^+ ions. This is illustrated in Figure 3b, which displays the $Cl^- \cdots O2$ pair RDFs. Consistently, the profiles obtained for the other $Cl^- \cdots O\#$ pair RDFs (not shown) indicated that Cl^- ions do not interact with the carbonyl groups of the UPEA-Phe chains, independently of the CLD. It should be mentioned that, although the RDFs were displayed

at short distances due to the inhomogeneity of the system, all them tend to converge to unity as expected, at $r = L/2$ (where L is the size of the simulation box).

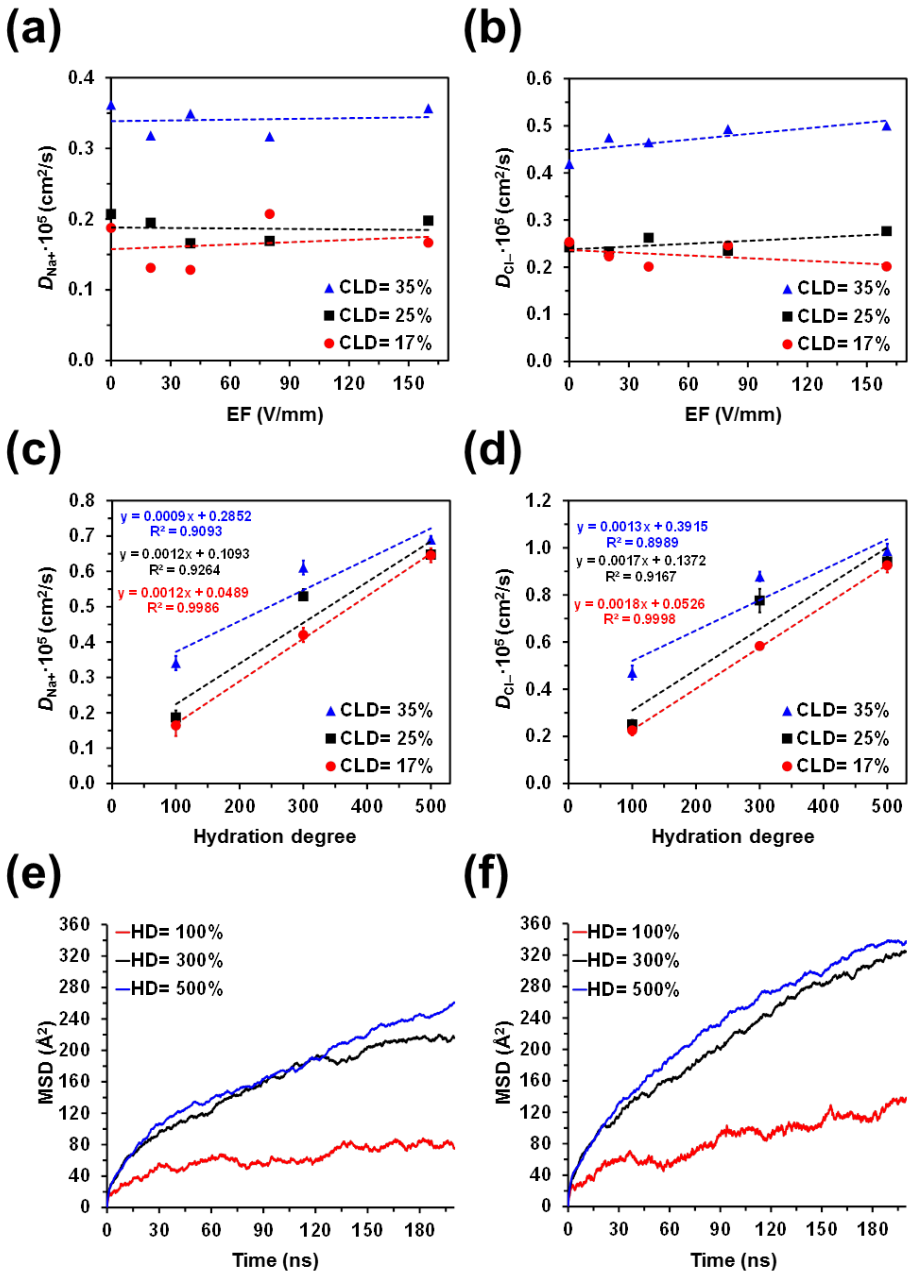

Figure 2. Variation of the diffusion coefficients of (a, c) Na^+ and (b, d) Cl^- (D_{Na+} and D_{Cl-}, respectively) against: (a, b) the strength of the electric field for UPA-Phe hydrogels with HD= 100% (*i.e.* profiles for hydrogels with HD= 300% and 500% are shown in Figure S1); and (c, d) the hydration degree. For hydrogels displayed in (a)-(d), the plotted diffusion

coefficients correspond to the averages of the values obtained using different electric fields, while the error bars are to the resulting standard deviations. Temporal evolution of the MSD for (e) Na^+ and (f) Cl^- ions in the hydrogel with CLD= 25% using EF= 20 V/mm (results for the systems with CLD= 17% and 35% are shown in Figure S4).

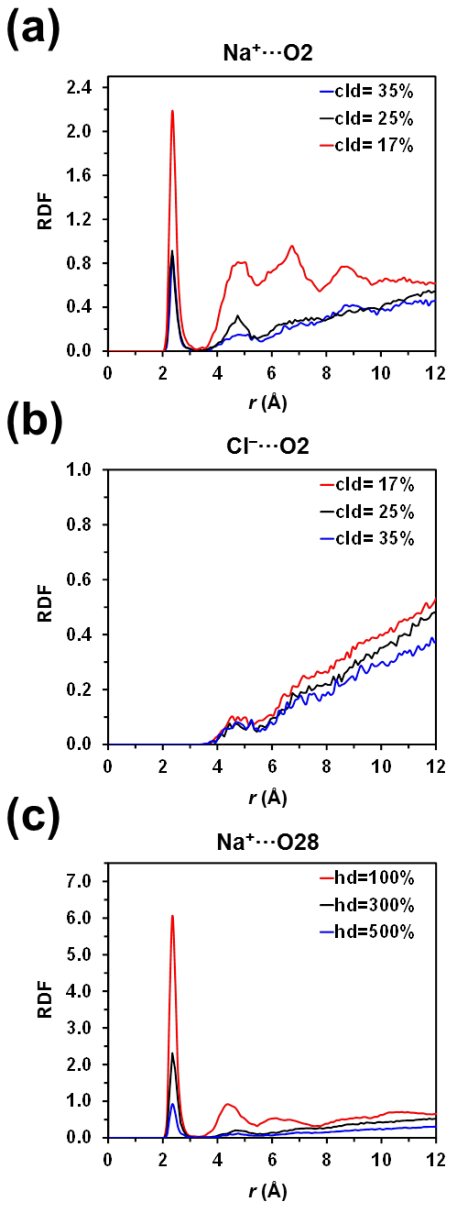

Figure 3. Radial distribution functions (RDF) for (a) Na^+···O2 and (b) Cl^-···O2 atom pairs, as determined from simulations of hydrogels with different cld and hb= 100%, and for (c)

$Na^+\cdots$O28 atom pairs, as obtained from simulations of hydrogels with different hd and cld= 17%.

Figure 2c-d plots the variation of D_{Na+} and D_{Cl-}, respectively, against the HD for the three hydrogels for EF= 20 V/mm. Both D_{Na+} and D_{Cl-} increase linearly with the HD, indicating that the mobility of the ions becomes easier with increasing water content. This effect is clearly illustrated in Figure 2e-f, which displays the temporal evolution of the MSD for representative simulations (EF= 20 V/mm) of systems with CLD= 25% (the temporal evolution of the MSD for the systems with CL= 17% and CLD= 35% are shown in Figure S4). Thus, the amount of $Na^+\cdots$UPEA-Phe interactions and, therefore, the retention of Na^+ cations bound to the hydrogel matrix decreases with increasing HD. The linear increment of the diffusion coefficients with the HD has been attributed to the fact that ion$\cdots$polymer interactions are relatively weak and non-specific in comparison to ion$\cdots$water interactions. This effect is illustrated in Figure 3c, which compares the RDFs involving the $Na^+\cdots$O28 pair for the hydrogels with CLD= 17% and variable water contents, and supported by the RDFs shown in Figure S3 for $Na^+\cdots$O2, $Na^+\cdots$O8 and $Na^+\cdots$O42 pairs. D_{Cl-} is higher than D_{Na+} for all the examined hydration degrees, which is due to the lack of specific interactions between Cl^- ions and UPEA-Phe atoms. It is worth noting that the chemical structure of hydrogels plays a crucial role in the diffusion coefficient for ions. For example, in ionene hydrogels (*i.e.* polyelectrolyte hydrogels in which a quaternary ammonium cation resides within the polymer backbone) the strong electrostatic interactions between the positively charged nitrogen atoms and ions dominate over the ion$\cdots$water interactions.[47,48]

The growing diffusion of the ions with the HD becomes more pronounced with decreasing CLD. Thus, the ratio between the D_{Na+} values obtained for HD= 500% and 100%, D_{Na+}(HD= 500%) / D_{Na+}(HD=100%), is 3.9, 3.5 and 2.0 for CLD= 17%, 25% and 35%, respectively. Similarly, D_{Cl-}(HD= 500%) / D_{Cl-}(HD=100%) is 4.1, 3.8 and 2.1 for CLD= 17%, 25% and 35%, respectively. These results are consistent with the amount of specific interactions between Na^+ ions and UPEA-Phe atoms, which increase with decreasing CLD (Figures 3a and S3), and with the fact that the migration of Cl^- is faster than that of Na^+.

On the other hand, both D_{Na+} and D_{Cl-} increase with the CLD, as is reflected in Figure 4a-b, respectively. However, this tendency is less pronounced for systems with HD= 500% than for those with HD= 100% and 300%. Again this is consistent with the amount of $Na^+\cdots$UPEA-Phe interactions, which is inversely proportional to the HD (Figures 3c and S2). The temporal evolution for the trajectories obtained using HD= 300% and 500% (EF= 20 V/mm) are shown in Figure 4c-d and 4e-f, respectively.

In summary, MD simulations show that Na^+ and Cl^- ions diffusion increases with the size of the pores, this structural parameter being indeed much more important than the strength of the electric field. This has inspired us to further improve the already outstanding properties of UPEA-Phe/NaCl as supporting electrolyte for ESCs, increasing the pore size. Because of the limitations typically found in the construction of crosslinked polymeric models, MD simulations were conducted using relatively low CLDs (*i.e.* CLD ≤ 35%), in which the pore size of modeled hydrogels increased with the CLD. However, in the laboratory, the size of the pore of real photo-crosslinked UPEA-Phe/NaCl hydrogels is expected to be increased by reducing the time of exposure to UV radiation from 8 h, which

ensured that the crosslinking reaction was completed, to 4 h. Experimental measures about the performance of UPhe-Phe/NaCl hydrogels prepared using such two photo-polymerization times are provided in the next section.

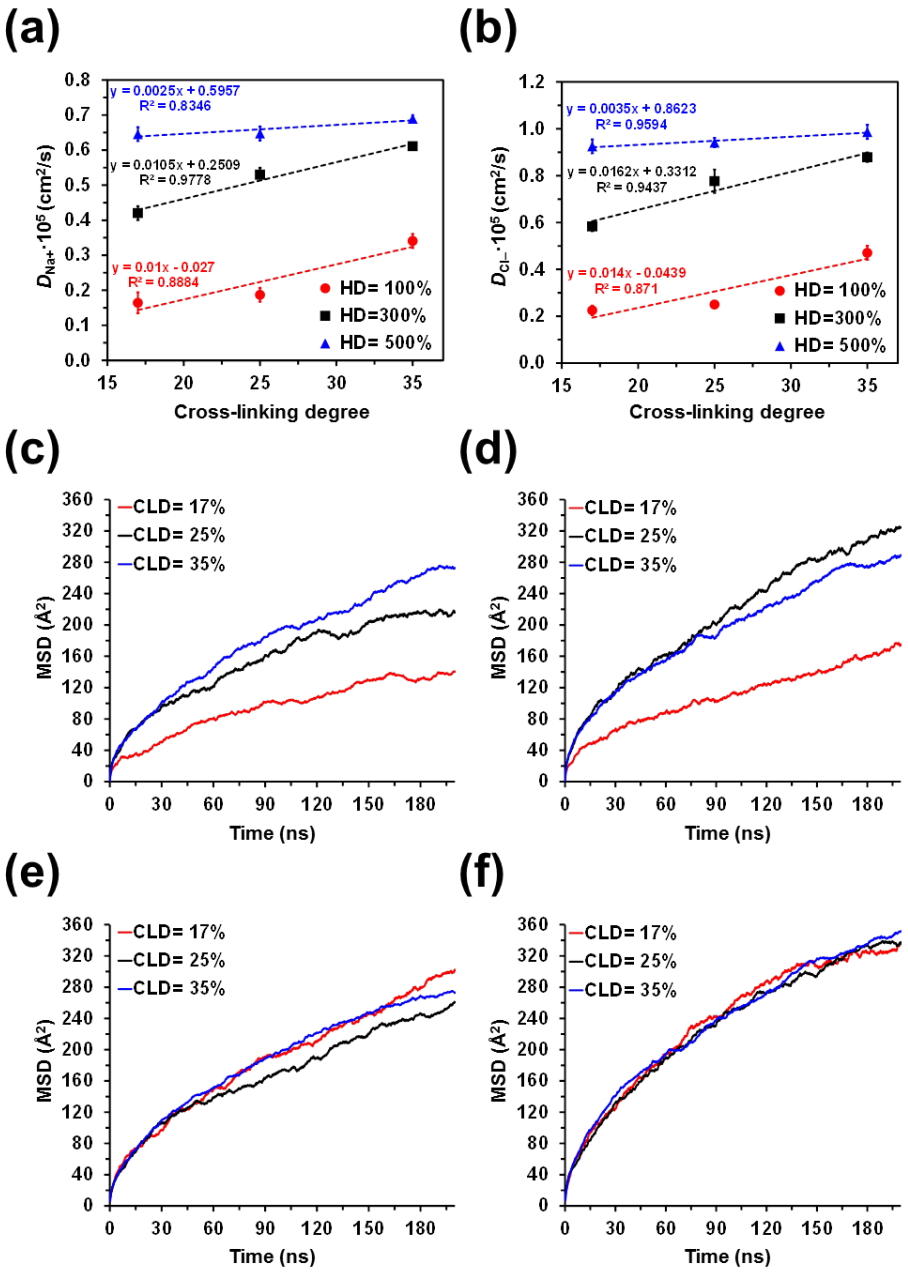

Figure 4. Variation of the diffusion coefficients of (a) Na^+ and (b) Cl^- (D_{Na+} and D_{Cl-}, respectively) against the cross-linking degree. The plotted diffusion coefficients correspond to the averages of the values obtained using different electric fields, while the error bars are

to the resulting standard deviations. The temporal evolution of the MSD for (c, e) Na^+ and (d, f) Cl^- ions in the hydrogels with (c, d) HD= 300% and (e, f) HD= 500% using EF= 20 V/mm.

Experimental characterization of UPEA-Phe/NaCl as solid electrolyte

UPEA-Phe hydrogels were prepared as described in previous work.[35] In brief, UPEA-Phe chains were obtained following the procedure reported by Katsarava and co-workers.[49] Then, UPEA-Phe chains were crosslinked using as reticulating agent a functionalized PEG (M_n= 10000 g/mol), which was obtained by reacting with 2-propenoyl chloride.[35] The crosslinking reaction between UPEA-Phe and the functionalized PEG was performed using the photo-initiator irgacure 2959 and exposing the reaction medium solution to an UV lamp (230 V, 0.8 A). Two photo-polymerization times (*i.e.* times of exposure to the UV radiation) were considered: 4 h and 8 h. The latter time ensured that the crosslinking reaction was completed, as proved in previous work.[35] Therefore, the resulting hydrogel was used as a control. Instead, the choice of the shortest time was based on the computational results discussed in the previous section. Thus, such drastic reduction of photo-polymerization time (a factor of two) was expected to promote the formation of larger pores since the reticulation process was interrupted before it was completed. Hydrogels obtained using times of 4 h and 8 h, hereafter named UPEA-Phe(4h) and UPEA-Phe(8h), were washed at room temperature with distilled water, which was changed every 12 h, during 48 h. Finally, the hydrogels were soaked a minimum of 24 h in a 0.1 M NaCl solution prepared with distilled water for doping. The doped hydrogels, UPEA-Phe(4h)/NaCl and UPEA-Phe(8h)/NaCl, were kept in such NaCl solution for future

utilization or lyophilized by freeze-drying for further characterization. Figure 5a provides photographs of the UPEA-Phe(4h) hydrogel as prepared and after doping with NaCl.

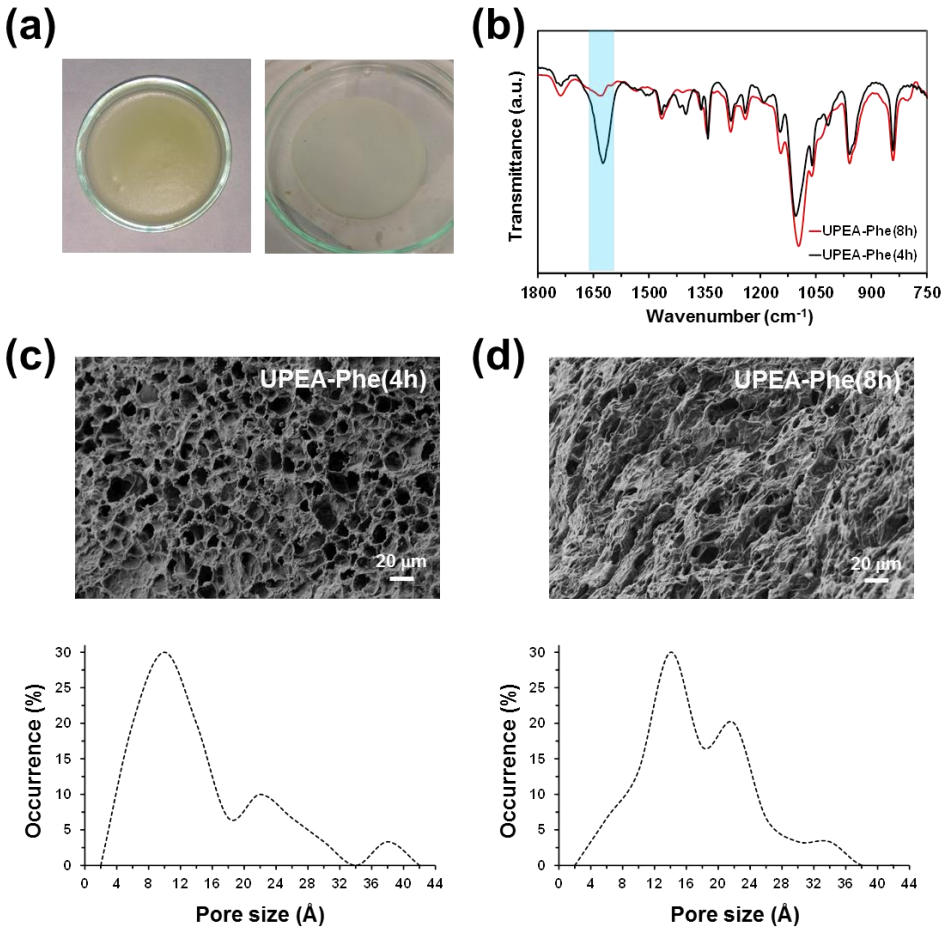

Figure 5. (a) Photographs of washed UPEA-Phe(4h) and doped UPEA-Phe(4h)/NaCl. (b) FTIR spectra of freeze-dried hydrogels. The band associated to the C=C stretching is marked in blue. Representative SEM micrographs and pore size distribution for freeze-dried (c) UPEA-Phe(4h) and (d) UPEA-Phe(8h) hydrogels.

The FTIR spectra of UPEA-Phe(4h) and UPEA-Phe(8h), which have been normalized using the most intense band at 1100 cm^{-1} (C–O stretching), are compared in Figure 5b. As expected, the main difference between the two compounds corresponds to the band at 1620 cm^{-1}, which is associated to the C=C stretching. The intensity of this band decreases with

increasing CLD (*i.e.* with increasing photo-polymerization time). The rest of the FTIR bands, as well as the ^{1}H NMR spectra (not shown), are fully consistent with those described in previous work.[35]

On the other hand, representative SEM micrographs of freeze-dried UPEA-Phe(4h) and UPEA-Phe(8h) are shown in Figure 5c-d. Pores are much better defined in the former than in latter. In fact, UPEA-Phe(8h) shows some compact regions homogeneously distributed on the surface, in which the pores are totally or practically hindered. This effect has been attributed to the fact that the photo-polymerization reaction was complete after 8 h. Interestingly, the average size of the pores that remain open in UPEA-Phe(8h), 17±7 μm, is slightly higher than that of the UPEA-Phe(4h) pores, 14±10 μm, even though a higher dispersion of values is obtained for the latter. This observation, which is reflected in the distribution of sizes included in Figure 5c-d, indicates that the continuation of the photo-polymerization process for 4 additional hours mainly affects the smaller pores, suggesting that functionalized PEG tend to be grouped in micro/nanoclusters rather than homogeneously distributed in the reaction medium.

The swelling ratio (*SR*, %) of the two hydrogels was estimated using the weights of the hydrogels after washing and after freeze-drying (ESI). The *SR* was 1501 % ± 342% and 500% ± 114 % for UPEA-Phe(4h) and UPEA-Phe(8h), respectively, reflecting that this parameter decreases with increasing CLD as was also observed for other polysaccharide- and polypeptide-based hydrogels.[33,34]

To compare the electrochemical achievements of UPEA-Phe(4h)/NaCl and UPEA-Phe(8h)/NaCl as solid electrolytes, ESCs devices were prototyped by assembling such doped hydrogels with poly(3,4-ethylenedioxythiophene) (PEDOT) electrodes, as is

illustrated in Figure 6a. More specifically, a rectangular hydrogel piece was sandwiched between two PEDOT electrodes, separated at a distance of 1 mm. After this, the external side of each PEDOT electrodes was covered by another hydrogel piece. A photograph of the resulting ESC prototype is included in Figure 6a. It is worth noting that the choice of PEDOT electrodes, which consisted on steel sheets coated at the two sides by anodically polymerized PEDOT (detailed description of the preparation and characterization of the electrodes is provided in the ESI), and the two-electrodes configuration was done for consistency with previous studies in which other hydrogels were tested.[31-35] This has allowed us to stablish a rigorous comparison with hydrogels derived from biopolymers, showing the remarkable performance of UPEA-Phe(4h)/NaCl as solid and flexible electrolyte (see last sub-section).

Figure 6b shows the cyclic voltammetry (CV) curves of ESCs with UPEA-Phe(4h)/NaCl and UPEA-Phe(8h)/NaCl recorded at different scan rates (from 10 to 200 mV/s) and a working potential from 0.0 to 0.8 V. For each scan rate, the areas associated to the cathodic and anodic scans are significantly higher for UPEA-Phe(4h)/NaCl than for UPEA-Phe(8h)/NaCl, indicating that the reversible exchange of voltammetric charge is favored for the former hydrogel. Moreover, voltammograms at low scan rates exhibit a rectangular shape, reflecting the pseudo-capacitive behavior associated to the formation of the electrochemical double layer at the electrode/electrolyte interface. As the scan rate increases, voltammograms deviate from the rectangular shape for both ESCs. However, this effect is much less pronounced for UPEA-Phe(4h)/NaCl than for UPEA-Phe(8h)/NaCl, revealing better ionic diffusion for the former than for the latter.

Galvanostatic charge-discharge (GCD) curves at different current densities are displayed in Figure 6c. UPEA-Phe(4h)/NaCl-containing ESCs show lower voltage drop than those

with UPEA-Phe(8h)/NaCl, independently of the current density, indicating that the internal resistance is lower for the former than for the latter. GCD triangular curves are more symmetric when more capacitive is the behavior due to symmetry in charge and discharge (*i.e.* coulombic efficiency close to one*)*. Compared with those of UPEA-Phe(8h)/NaCl, the shape of the GCD curves of UPEA-Phe(4h)/NaCl is closer to the ideal symmetric triangular profiles. This is consistent with the fact that electric double layer capacitive behavior is better for ESCs containing the latter solid electrolyte, which is in agreement with CV results. Another important finding is that charge and discharge times are almost twice for the ESCs with UPEA-Phe(4h)/NaCl than for the ESC with UPEA-Phe(8h)/NaCl.

Figure 6d represents the specific capacitances (*SC*s) obtained from CV at various scan rates (from 10 to 200 mV/s) and from GCD at various current densities (from 0.43 to 2.44 A/g). In all cases, the *SC*s obtained for ESCs with UPEA-Phe(4h)/NaCl ESCs are higher than for those with UPEA-Phe(8h)/NaCl, reflecting again that the ionic diffusion is higher for the hydrogel with largest pores. Moreover, the difference between the specific capacitances of the two systems (*i.e.* $\Delta SC = SC_{\text{UPEA-Phe(4h)/NaCl}} - SC_{\text{UPEA-Phe(8h)/NaCl}}$) increases from 15.6 to 28.1 F/g when the scan rate increases from 10 to 200 mV/s, whereas ΔSC decreases from 19.8 to 2.9 F/g when the current density increases from 0.43 to 2.44 A/g. The latter observation indicates that the ions fully diffuse inside the electrodes at low current densities, this effect being enhanced for the hydrogel electrolyte with more available surface. As shown in Figure 6d, the *SC*s are higher for Phe(4)/NaCl hydrogel-containing ESCs than for control ESCs, which were prepared using PEDOT electrodes separated by a 0.5 M NaCl liquid solution, evidencing that the capacitive response was better for the former than for the latter.

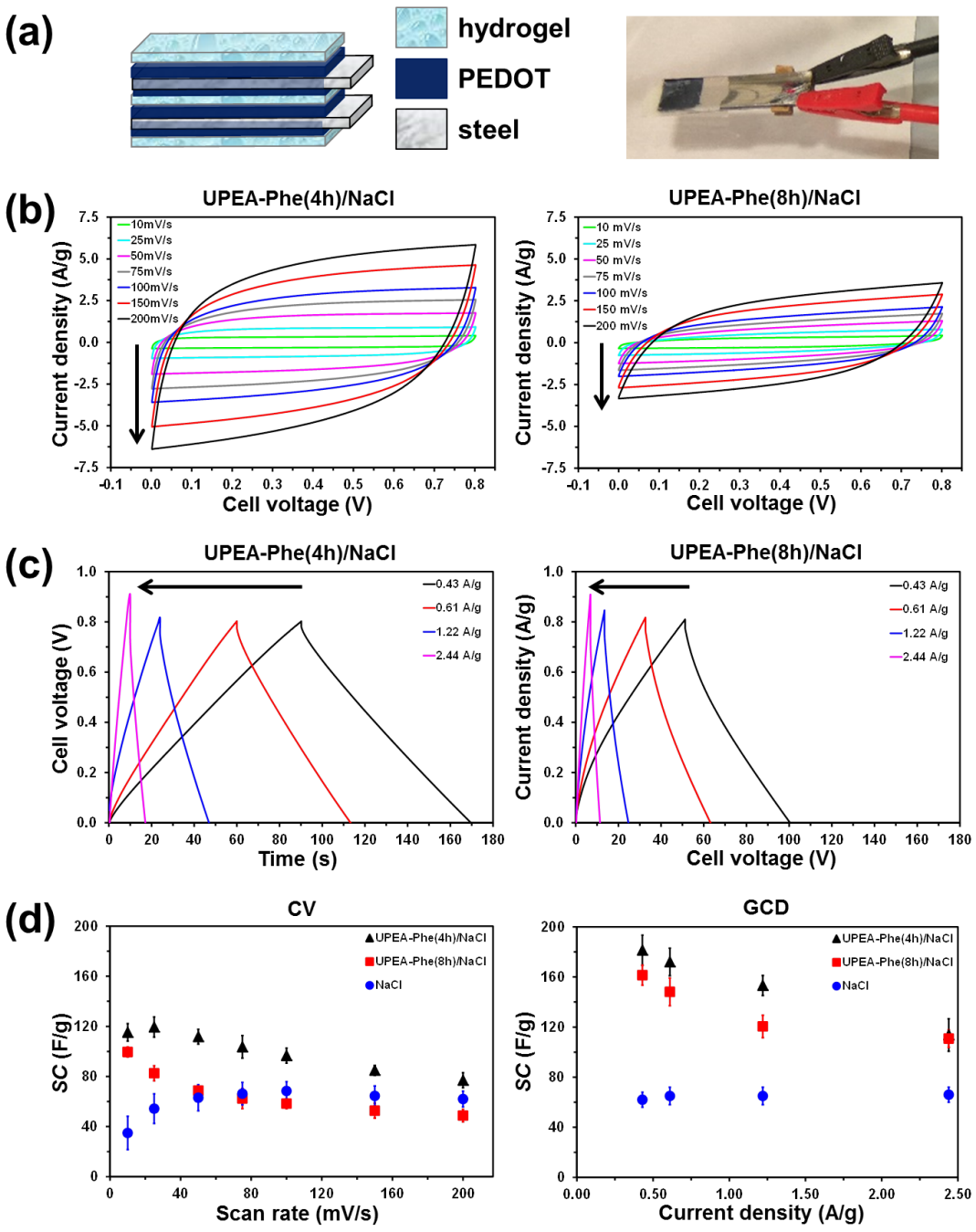

Figure 6. (a) Scheme and photograph of the ESC prepared in this work. For ESCs prepared using UPEA-Phe(4h)/NaCl and UPEA-Phe(8h)/NaCl: (b) Cyclic voltammograms recorded at different scan rates; (c) GCD curves recorded at different current densities; (d) *SC*s obtained by CV at different scan rates (left) and *SC*s obtained by GCD at different current densities. For comparison, *SC*s obtained using ESCs with a liquid electrolyte (0.5 M NaCl) are included in (d).

The UPEA-Phe(4h)/NaCl-containing ESC shows a Coulombic efficiency (η) that grows marginally, from 90% to 92%, when the current density increases from 0.43 to 2.44 A/g as compared with the more important reduction from 92% to 78% for the ESC with UPEA-Phe(8h)/NaCl (Figure 7a). These variations indicate that the 3D structure of the UPEA-Phe(4h) hydrogel is more appropriate to preserve the reversibility in ion diffusion processes than that of UPEA-Phe(8h) one. Indeed the low η obtained for the UPEA-Phe(8h)/NaCl-containing ESC at the highest current density (78%) should be attributed to the partial broken up of the diffusion paths for ions.

The self-discharge profiles, which represent the spontaneous voltage decay on a charged ESC after a set period of time, are compared in Figure 7b. For this assay, ESCs were charged to 0.80 V at 0.50 mA, maintained at $1 \cdot 10^{-1}$ mA for 10 min and, finally, discharged to 0.00 V at -1.00 mA. The end cell voltage, which was around 0.5 V, and the short-term self-discharging time was very similar for both UPEA-Phe(8h)/NaCl and UPEA-Phe(4h)/NaCl ESCs. Thus, the main difference occurs at the charging process that is faster for the former than for the latter, which is consistent with GCD assays (Figure 6c). In any case, the fact that both ESCs present a final voltage over 0.5 V, indicating a retention >60% in the short term, ensures specific practical applications.

On the other hand, the leakage current of the two devices, which are compared in Figure 7c show a significant dropping in the beginning followed by a gradual stabilization. For UPEA-Phe(4h)/NaCl-containing ESCs, the leakage current is of 99 and 93 μA after 150 and 600 s, respectively, whereas for ESCs with UPEA-Phe(8h)/NaCl is 23 and 13 μA after 150 and 600 s, respectively. Although such low values of leakage current, which are

ascribed to the self-discharge course in the device, mean that shuttle reactions caused by the impurities at the electrode materials are very small, leakage is slightly prevented when the crosslinking is not complete.

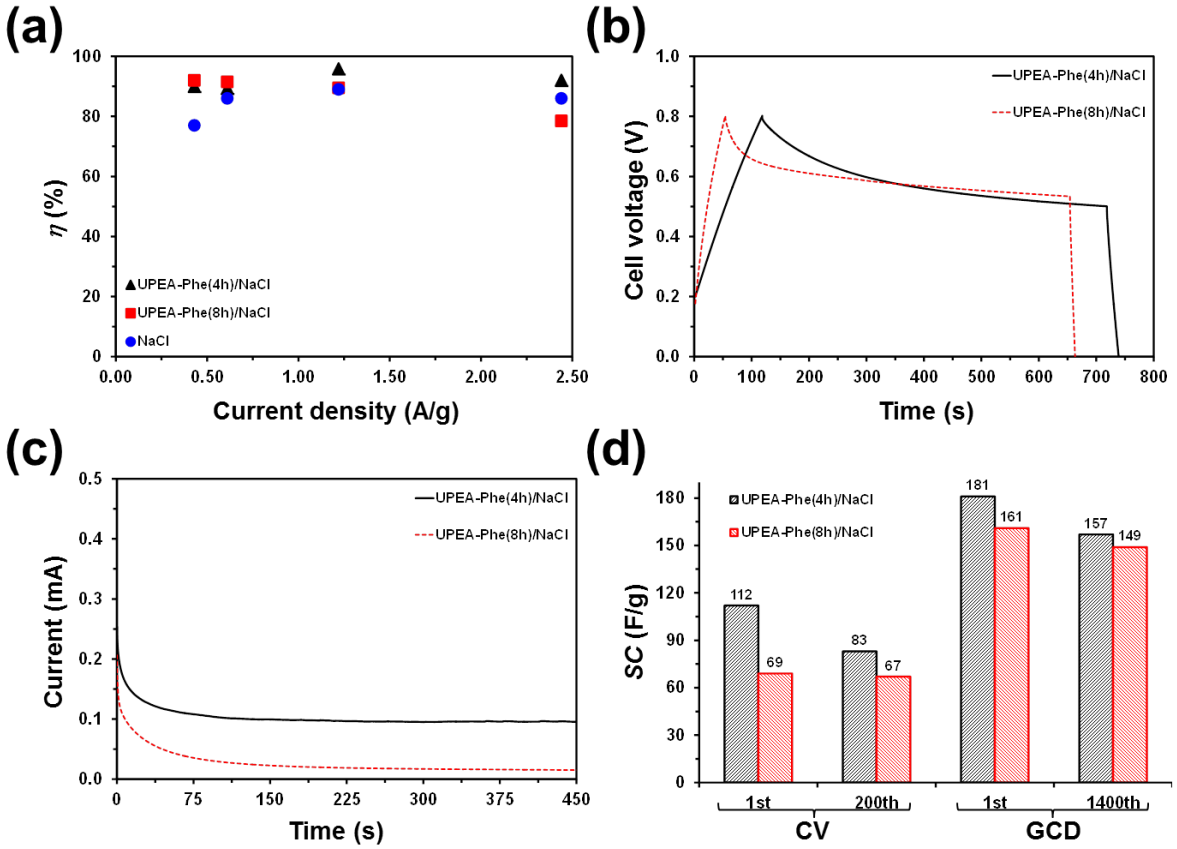

Figure 7. For ESCs with UPEA-Phe(4h)/NaCl and UPEA-Phe(8h)/NaCl: (a) Variation of the Coulombic efficiency (η) against the current density; (b) self-discharge; (c) leakage current curves; and (d) *SC*s after 200 consecutive CV cycles at 50 mV/s and after 1400 consecutive GCD cycles at 1.22 A/g. For comparison, the η values obtained using an ESC with a liquid electrolyte (0.5 M NaCl) are included in (a).

Cycling stability was evaluated considering 200 CV cycles at a scan rate of 50 mV/s and 1400 charge-discharge cycles at a current density of 1.22 A/g. The capacitance retention of two ESCs is compared in Figure 7d. The ESC with UPEA-Phe(8h)/NaCl exhibits higher capacitance retention (97% and 93% for CV and GCD, respectively) than the one with

UPEA-Phe(4h)/NaCl (74% and 87% for CV and GCD, respectively). The relatively low capacitance retention of the latter has been attributed to some structural changes underwent by the hydrogel electrolyte, which make more difficult the access and escape of dopant ions. Thus, the structural integrity of the hydrogel increases with the time of exposure to UV radiation. In spite of this, it is worth noting that the *SC* of device with UPEA-Phe(4h)/NaCl after 200 redox cycles and after 1400 charge-discharge cycles is higher than that of the ESC with pristine UPEA-Phe(8h)/NaCl (*i.e.* before starting the stability assays). This observation indicates that the lower of structural integrity in UPEA-Phe(4h) is compensated by higher available surface for ion diffusion.

It should be mentioned that UPEA-Phe hydrogels were also prepared using times of exposure to UV radiation of 2 and 6 h, named UPEA-Phe(2h) and UPEA-Phe(6h), respectively. The mechanical integrity of UPEA-Phe(2h) was very poor in comparison to that of UPEA-Phe(4h), requiring careful handling and, therefore, limiting its applicability as hydrogel electrolyte for ESCs. Instead, preliminary assays using ESCs constructed with UPEA-Phe(6h) showed a behavior close to those containing UPEA-Phe(8h), suggesting that, as expected, the photo-crosslinking reaction was very advanced after 6 h of exposure to UV radiation.

Comparison with other PEDOT-based ESCs

Figure 8 compares the performance of different ESCs devices that were all fabricated using PEDOT electrodes identical to the ones employed in the present work combined with different solid and liquid electrolytes. Accordingly, differences in their behaviors can be exclusively attributed to the electrolyte. Among solid electrolytes, UPEA-Phe(4h)/NaCl and UPEA-Phe(8h)/NaCl have been compared with the following doped hydrogels: *a)*

poly-γ-glutamic acid hydrogel doped with $NaHCO_3$ in which polypeptide chains were covalently crosslinked using cystamine;[34] *b)* carboxymethyl cellulose hydrogel crosslinked with citric acid and doped with NaCl;[33] *c)* carboxymethyl cellulose sodium salt paste, which consists in an extremely high viscous polysaccharide aqueous solution, doped with NaCl;[33] and *d)* κ-carrageenan hydrogel, formed by adding KCl to a hot biopolymer aqueous solution, and doped with NaCl.[31] On the other hand, PEDOT-based ESCs with the following two liquid electrolytes were used for comparison: *i)* a phosphate buffer saline (PBS) solution;[33] and *ii)* a 0.5 M NaCl aqueous solution.[31]

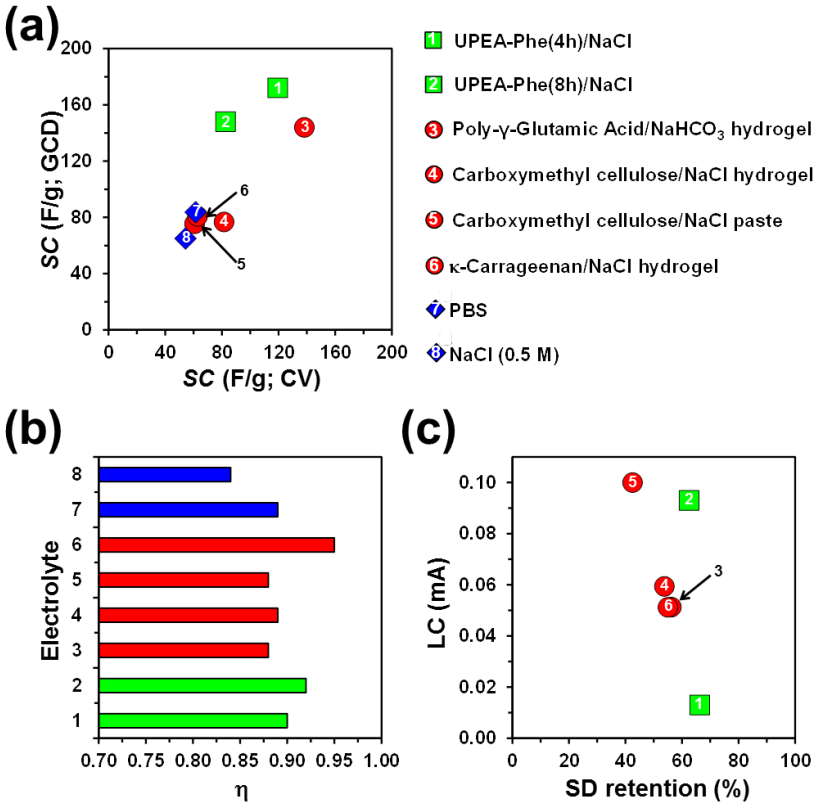

Figure 8. (a) *SC* map comparing the values obtained by CV (25 mV/s) and GCD (0.61 A/g) for different ESCs that only differ in the electrolyte (the number used to label the different solid and liquid electrolytes is displayed at the right). (b) Coulombic efficiency, as determined by GCD at 0.61 A/g, and (c) representation of the voltage retention (in %) by self-discharging against the leakage current for the same ESCs. The values compared in the

different graphics were measured considering identical experimental set-ups and conditions for all ESCs.

Figure 8a shows the capacitive map of the different ESCs, in which the *SC*s obtained by CV at 25 mV/s are represented against the *SC*s by GCD at 0.61 A/g. The highest GCD value corresponds to the UPEA-Phe(4h)/NaCl-containing ESC, whereas CV value of the latter is only surpassed by the device with poly-γ-glutamic acid/$NaHCO_3$. Interestingly, the performance of UPEA-Phe(8h)/NaCl as solid electrolyte is much better than those of carboxymethyl cellulose/NaCl paste and both κ-carrageenan/NaCl and carboxymethyl cellulose/NaCl hydrogels, the latter three exhibiting a *SC* values similar to that of liquid electrolytes. Figure 8b represents the Coulombic efficiencies, as determined by GCD at 0.61 A/g. The efficiencies of the two UPEA-Phe/NaCl hydrogels are only exceeded by the one of κ-carrageenan/NaCl. Indeed, the efficiency of carboxymethyl cellulose- and poly-γ-glutamic acid-containing devices is lower than that of the ESC with PBS as liquid electrolyte.

Figure 8c plots the voltage retention (in %) after applying a self-discharging test that was identical for all compared ESCs, against the leakage current. The highest end cell voltage retention is observed for the ESC with UPEA-Phe(4h)/NaCl. Moreover, the voltage retention of devices with the polypeptide/$NaHCO_3$ and carboxymethyl cellulose/NaCl is lower than the one of UPEA-Phe(8h)/NaCl by at least 6%. On the other hand, UPEA-Phe(4h)/NaCl presents the lowest leakage current, the parasitic current obtained for devices constructed with the other electrolytes being significantly higher. Because of its internal resistance, ESCs need a small current (the leakage current) to retain the cell voltage. Accordingly, Figure 8c allows us to conclude that the influence of the UPEA-Phe(4h)/NaCl

electrolyte on the internal resistance of the whole ESC, which should be dominated by the two PEDOT electrodes, is much lower than those exerted by the other hydrogels.

Conclusions

In summary, molecular simulations of doped UPEA-Phe hydrogels have shown that the diffusion coefficients of Cl^- and, especially, of Na^+ increase linearly with the size of the pore. Moreover, this effect is also influenced by the hydration degree since the amount of $Na^+\cdots$UPEA-Phe interactions is inversely proportional to the hydration degree. Simulations indicate that a hydration degree of at least 300% is recommendable for the transport of the ions. Simulation results have been used to design doped UPEA-Phe hydrogels with higher pore size than those reported in previous work.[35] For this purpose, the exposure to UV radiation has been reduced from 8 h to 4 h. By taking advantage of the reduction of the pore size and structure, the ion migration improves considerably. More specifically, the *SC* determined by CV increases 54% in average (from 16% to 66%, depending on the scan rate), while the *SC* obtained by GCD increases 14% (from 3% to 27%, depending on the current density). Another parameter that experiences a drastic improvement is the leakage current, which decreases one order of magnitude with increasing pore size. As a result, the electrochemical parameters achieved by ESCs prepared using UPE-Phe(4h)/NaCl as electrolyte are outstanding not only with respect to liquid electrolytes, but also with respect to other biodegradable and biocompatible doped hydrogels based on polypeptides and polysaccharides, when identical electrodes and experimental conditions are compared. These results strongly that the UPEA-Phe(4h)/NaCl proposed here can be extended to the

construction of a wide range of biocompatible, biodegradable and flexible energy-storage devices.

Conflicts of interest

There are no conflicts to declare.

Acknowledgements

Authors acknowledge MINECO/FEDER (RTI2018-098951-B-I00 and RTI2018-101827-B-I00) and the Agència de Gestió d'Ajuts Universitaris i de Recerca (2017SGR359 and 2017SGR373) for financial support. Support for the research of C.A. is grateful to ICREA Academia program for excellence in research.

References

1. D. P. Dubal, N. R. Chodankar, D.-H. Kim and P. Gómez-Romero, *Chem. Soc. Rev.*, 2018, **47**, 2065–2129.
2. Z. Bao and X. Chen, *Adv. Mater.*, 2016, **22**, 4177–4179.
3. M. M. Pérez-Madrigal, M. G. Edo and C. Alemán, *Green Chem.*, 2016, **18**, 5930–5956.
4. K. Xiao, L.-X. Ding, G. Liu, H. Chen, S. Wang and H. Wang, *Adv. Mater.*, 2016, **28**, 5997−6002.
5. L. Kou, T. Huang, B. Zheng, Y. Han, X. Zhao, K. Gopalsamy, H. Sun and C. Gao, *Nat. Commun.*, 2014, **5**, 3754.
6. P. Yang and W. Mai, *Nano Energy*, 2014, **8**, 274−290.

7. Z. F. Zhang, X. R. Su, Y. Y. Zhu, Z. H. Chen, Z. B. Fang and X. J. Luo, *Nanoscale*, 2019, **11**, 16071−16079.
8. Y. P. Huang, F. Cui, J. Bao, Y. B. Zhao, J. X. Lian, T. X. Liu and H. M. Li, *J. Mater. Chem. A*, 2019, **7**, 20778−20789.
9. Y. H. Zhang, Z. Shang, M. X. Shen, S. P. Chowdhury, A. Ignaszak, S. H. Sun and Y. H. Ni, *ACS Sustain. Chem. Eng.*, 2019, **7**, 11175−11185.
10. G. B. Lou, Y. T. Wu, X. Q. Zhu, Y. Z. Lu, S. Yu, C. H. Yang, H. Chen, C. Guan, L. Li and Z. H. Shen, *ACS Appl. Mater. Interfaces*, 2018, **10**, 42503−42512.
11. P. Sundriyal and S. Bhattchraya, *ACS Appl. Mater. Interfaces*, 2017, **9**, 38507−38521.
12. M. C. G. Saborío, S. Lanzalaco, G. Fabregat, J. Puiggalí, E. Estrany and C. Aleman, *J. Phys. Chem. C*, 2018, **122**, 1078–1090.
13. G. F. Cai, P. Darmawan, M. Q. Cui, J. X. Wang, J. W. Chen, S. Magdassi and P. S. Lee, *Adv. Energy Mater.*, 2016, **6**, 1501882.
14. G. Wang, X. Sun, F. Lu, H. Sun, M. Yu, W. Jiang and C. Liu, *Small*, 2011, **8**, 452–459.
15. X. Lu, M. Yu, G. Wang, Y. Tong and Y. Li, *Energy Environ. Sci.*, 2014, **7**, 2160–2181.
16. J. Yu, W. Lu, S. Pei, K. Gong, L. Wang, L. Meng, Y. Huang, J. P. Smith, K. S. Booksh, Q. Li, J.-H. Byun, Y. Oh, Y. Yan and T.-W. Chou, *ACS Nano*, 2016, **10**, 5204−5211.
17. X. Wang, B. Liu, R. Liu, Q. Wang, X. Hou, D. Chen, R. Wang and G. Shen, *Angew. Chem., Int. Ed.*, 2014, **53**, 1849−1853.

18. W. Li, F. Gao, X. Wang, N. Zhang and M. Ma, *Angew. Chem., Int. Ed.*, 2016, **55**, 9196−9201.

19. Y. Guo, X. Zhou, Q. Tang, H. Bao, G. Wang and P. Saha, *J. Mater. Chem. A*, 2016, **4**, 8769−8776.

20. Y. Huang, M. Zhong, Y. Huang, M. Zhu, Z. Pei, Z. Wang, Q. Xue, X. Xie and C. Zhi, *Nat. Commun.*, 2015, **6**, 10310.

21. X. Liu, D. Wu, H. Wang and Q. Wang, *Adv. Mater.*, 2014, **26**, 4370−4375.

22. X. Liu, C. Yin, J. Yang, M. Liang, J. Wei, Z. Zhang, H. Wang and Q. Wang, *J. Mater. Chem. A*, 2016, **4**, 17933−17938.

23. H. Z. Yang, Y. Liu, L. B. Kong, L. Kang and F. Ran, *J. Power Sourc.*, 2019, **426**, 47−54.

24. Z. Z. Sun, F. Li, D. Zhang and W. L. Song, *J. Electrochem. Soc.*, 2018, **165**, H820−H830.

25. Z. Y. Peng, Y. B. Zou, S. Q. Xu, W. B. Zhong and W. T. Yang, *ACS Appl. Mater. Interfaces*, 2018, **10**, 22190−22200.

26. L. Fu, A. W. Wang, F. C. Luy, G. S. Lai, J. H. Yu, C. T. Lin, Z. Liu, A. M. Yu and W. T. Su, *Sens. Actuators B*, 2018, **262**, 326−333.

27. J. Zhao, Y. Chen, Y. Yao, Z. R. Tong, P. W. Li, Z. M. yang and S. H. Jin, *J. Power Sourc.*, 2018, **378**, 603−609.

28. L. J. Cao, M. Y. Yang, D. Wu, F. C. Luy, Z. F. Sun, X. W. Zhong, H. Pan, H. T. Liu and Z. G. Lu, *Chem. Commun.*, 2017, **53**, 1615−1618.

29. P. R. Kasturi, H. Ramasamy, D. Meyric, Y. S. Lee and R. K. Selvan, *J. Colloid Interf. Sci.*, 2019, **554**, 142−156

30. E. Armelin, M. M. Pérez-Madrigal, C. Alemán and D. D. Díaz, *J. Mater. Chem. A*, 2016, **4**, 8952−8968.
31. M. M. Pérez-Madrigal, F. Estrany, E. Armelin, D. Díaz-Díaz and C. Alemán, *J. Mater. Chem. A*, 2016, **4**, 1792–1805.
32. G. Fabregat, L. Hodasova, L. J. del Valle, F. Estrany and C. Aleman, *Adv. Eng. Mater.*, 2018, **20**, 1800018.
33. M. M. Pérez-Madrigal, M. G. Edo, M. Saborío, F. Estrany and C. Alemán, *Carbohydr. Polym.*, 2018, **200**, 456–467.
34. M. M. Pérez-Madrigal, M. G. Edo, A. Díaz, J. Puiggalí and C. Alemán, *J. Phys. Chem. C*, 2017, **121**, 3182–3193.
35. G. Ruano, A. Díaz, J. Tononi, J. Torras, J. Puiggalí and C. Alemán, *Polym. Test.*, 2020, **82**, 106300.
36. F. Leontidis, B. Forrest, A. H. Widmann and U. W. Suter, *J. Chem. Soc., Faraday Trans.*, 1995, **91**, 2355–2368.
37. C. Alemán, N. Ch. Karayiannis, D. Curcó, K. Foteinopoulou and M. Laso, *J. Mol. Struct. (Theochem)*, 2009, **898**, 62–72.
38. O. Bertran, D. Curcó, J. Torras, C. A. Ferreira and C. Alemán, *Macromolecules*, 2010, **43**, 10521–10527.
39. D. Curcó and C. Alemán, *J. Comput. Chem.*, 2004, **25**, 790–798.
40. D. Curcó and C. Alemán, *J. Comput. Chem.*, 2007, **28**, 1743–1749.
41. J. Wang, W. Wang, P. A. Kollman and D. A. Case, *J. Mol. Graph. Model.*, 2006, **25**, 247–260.
42. J. Wang, R. M. Wolf, J. W. Caldwell, P. A. Kollman and D. A. Case, *J. Comput. Chem.*, 2004, **25**, 1157–1174.

43. N. J. English and C. J. Waldron, *Phys. Chem. Chem. Phys.*, 2015, **17**, 12407–12440.

44. S. Riniker, *J. Chem. Inf. Model.*, 2018, **58**, 565–578.

45. D. A. Case, I. Y. Ben-Shalom, S. R. Brozell, D. S. Cerutti, T. E. Cheatham III, V. W. D. Cruzeiro, T. A. Darden, R. E. Duke, D. Ghoreishi, M. K. Gilson, H. Gohlke, A. W. Goetz, D. Greene, R. Harris, N. Homeyer, S. Izadi, A. Kovalenko, T. Kurtzman, T. S. Lee, S. LeGrand, P. Li, C. Lin, J. Liu, T. Luchko, R. Luo, D. J. Mermelstein, K. M. Merz, Y. Miao, G. Monard, C. Nguyen, H. Nguyen, I. Omelyan, A. Onufriev, F. Pan, R. Qi, D. R. Roe, A. Roitberg, C. Sagui, S. Schott-Verdugo, J. Shen, C. L. Simmerling, J. Smith, R. Salomon-Ferrer, J. Swails, R. C. Walker, J. Wang, H. Wei, R. M. Wolf, X. Wu, L. Xiao, D. M. York and P. A. Kollman, AMBER 2018, University of California, San Francisco, 2018.

46. J. M. Bae, I. Honma, M. Murata, T. Yamamoto, M. Rikukawa and N. Ogata, *Solid State Ionics*, 2002, **147**, 189–194.

47. J. Bachl, D. Zanuy, D. E. López-Pérez, G. Revilla-López, C. Cativiela, C. Alemán and D. D. Díaz, *Adv. Funct. Mater.*, 2014, **24**, 4893–4904.

48. J. Bach, O. Bertran, J. Mayr, C. Alemán and D. D. Díaz, *Soft Matter*, 2017, **13**, 3031–3041.

49. K. Guo, C. C. Chu, E. Chkhaidze and R. Katsarava, *J. Polym. Sci.; Part A: Polym. Chem.*, 2005, **43**, 1463–1477.

Graphical abstract